Natural Resources for Human Health

eISSN: 2583-1194

Original Research

Received 16 May 2026
Revised 24 June 2026
Accepted 20 July 2026

Natural Resources for Human Health 2026, Vol. 6 (8s): 1372–1393

KEYWORDS:
Eugenol, Fagonia indica, $AgNO_3$, MTT assay, Caspase

Eugenol–AgNPs Induce Apoptosis and Upregulate Apoptosis -Related Caspase Gene Expression in MCF-7/C3 Breast Cancer Cells

Asseel Majeed Alamery[1], Fouad Razzaq Al-Burki[2], Asia Ali Hamza[3], Muder Al Haydar[4]

[1]College of Pharmacy, Jabir Ibn Hayyan University for Medical and Pharmaceutical Sciences, asseelmajeed6@gmail.com , https://orcid.org/0009-0004-7191-2231
[2]College of Pharmacy, Jabir Ibn Hayyan University for Medical and Pharmaceutical Sciences, fouad.razzaq@jmu.edu.iq , https://orcid.org/0000-0001-5016-5194
[3]College of Pharmacy, AlKafeel University, assia.ali@gmail.com
[4]College of Pharmacy, Jabir Ibn Hayyan University for Medical and Pharmaceutical Sciences, m.hayder@jmu.edu.iq , https://orcid.org/0000-0001-7008-4850

ABSTRACT: The purpose of this study was to assess the anticancer potential of Eugenol–AgNPs obtained from the extract of Fagonia indica and find out its mode of action on MCF-7/C3 breast cancer cells. GC-MS analysis revealed a total of 48 components, with Eugenol accounting for 26.45% of the relative peak area. In all of the analyses performed using HPLC-DAD method, the Eugenol peak constituted 26.6% of the total summation of peak area. The purity attained in the Eugenol-enriched fraction is about 94.7 ± 1.5%. The characterization of Eugenol–AgNPs was carried out using various techniques such as FTIR, UV–Vis, TEM/HRTEM, DLS, XRD, EDX, and zeta potential. The TEM/HRTEM analysis confirmed the existence of nanoparticles mostly in spherical shape with average size being 44.1 ± 6.7 nm. The hydrodynamic diameter as observed by DLS was 68.6 ± 5.4 nm. Overall characterization confirmed formation of Eugenol–AgNPs and its physicochemical properties including zeta potential, which was measured as −24.8 ± 2.9 mV. The nanoparticles showed strong dose-dependent cytotoxic effects against MCF-7/C3 cells with IC_{50} equal to 1.854 μg/mL. The analysis using Annexin V/PI demonstrated a significant increase in apoptotic cellsm while the RT-qPCR revealed increased in Caspase-3, Caspase-8, and Caspase-9 expression. Moreover, Eugenol-AgNPs has also been observed to have selectivity regarding the cytotoxicity of the MCF-7/C3 cells as compared to MCF-10A cells, where selectivity indexes of Eugenol-Ag noted to be 5.31. These collective data indicates that Eugenol-AgNPs have anti-breast cancer properties because of apoptosis induction. They appear to be a promising candidate for a plant-based nanocomposite that begs for more research to establish its clinical maximum.

1. INTRODUCTION

Breast cancer is the most prevalent cancer among women globally, and the MCF-7/C3 (estrogen-dependent) cell line is an excellent model for testing the efficacy of multiple anti-cancer drugs because of its similarity to human breast cancer cells (falling into the same subtype) (Giaquinto *et a*l., 2022). Plant compounds have shown to exhibit anti-cancer effects on MCF-7/C3 cells through various apoptotic pathways; however, the effectiveness of these compounds as therapies is hampered by their water insolubility, low absorption rates, and lack of accumulation in the target tissue (Gurunathan *et al.*, 2014; Hago *et al.*, 2023).

Cytotoxic activity against the MCF-7/C3 breast cancer cell line expressing estrogen receptor-positive cell line, is demonstrated by the ethanol extracts of Linum usitatissimum, Allium sativum, and Nigella sativa with IC50 concentrations of 2.008 ± 0.18, 8.661 ± 0.25, and 10.072 ± 0.18 μg/mL, respectively (Hago *et al.*, 2023).

Ongoing research into herbal medicines remains a key contributor to the identification of novel anticancer therapies. According to a report, since over half of FDA-approved antineoplastic drugs since 1985 have been natural, semi-synthetic or structural analogues of natural products (Newman and Cragg G, 2020). The variety of antiproliferative activities seen from the secondary metabolite class of compounds (phenolics, alkaloids, and flavonoids) can revolve significantly from batch-to-batch, requiring sufficient analyses to identify and isolate the most biologically-active constituents (e.g., chromatography) (Atanasov *et al.*, 2021; Harvey *et al.*, 2022).

Eugenol (4-allyl-2-methoxyphenol) is a prominent naturally occurring phenolic compound found primarily in the essential oils of several plants in the Lamiaceae, Myrtaceae, Lauraceae, and Myristicaceae families, particularly cloves (80–90%), giving it a pungent, clove-like aroma (Marchese *et al.*, 2017; Pires Costa *et al.*, 2025).

It is commonly used as a pain reliever and flavoring agent in cosmetics and food products. This compound also displays a broad range of pharmacological activities, notably antioxidant, anti-inflammatory, anticancer effects, antidiabetic, and antifungal properties (Murakami *et al.*, 2017; Kuo *et al.*, 2021). At the molecular level, evidence suggests that Eugenol exerts its antitumor effects by inducing apoptosis and inhibiting cancer cell proliferation, through the regulation of oxidative stress and its influence on mitochondrial pathways associated with cell survival (Kamatou *et al.*, 2012; Jaganathan and Supriyanto, 2012).

Regarding breast cancer, Eugenol has been shown to inhibit MCF-7/C3 cell growth in a dose-dependent manner. Some studies have reported an IC_{50} value of approximately 22.75 μM, accompanied by a significant enhanced intracellular ROS levels and disruption of mitochondrial membrane potential, leading to the induction of the intrinsic pathway of apoptosis (Noman *et al.*, 2025). Other studies have demonstrated that exposure to higher Eugenol concentrations (around 0.9 mM) results in decreased ATP levels and increased oxidative stress, leading to mitochondrial dysfunction and inducing cancer cell death. These findings support its role in regulating apoptosis-related gene expression, including increased Bax, decreased Bcl-2, and caspase activation, thus reinforcing its importance as a promising phenolic compound for targeting breast cancer (Jaganathan and Supriyanto, 2012; Ulanowska and Olas, 2021).

Analytical techniques such as GC–MS and HPLC are therefore essential for guiding compound isolation and improving biological reproducibility, frequently enhancing activity (Al-Burki, 2026). Research indicates that most of the biological activity of the isolated compounds obtained via GC–MS-guided fractionation will have been increased at least 2-5 times compared to the original extract, since these compounds are now concentrated with respect to molecules that have pharmacological activities (Said *et al.*, 2025; Sharma *et al.*, 2023; Salman *et al.*, 2026). In the same manner, high-performance liquid chromatography (HPLC) serves as an efficient technique for isolating target compounds from complicated matrices of natural products (Queiroz *et al.*, 2024; Salman *et al.*, 2026).

Nanotechnology delivery systems have proven to be a viable method of improving the problems related to free phytochemicals. Silver nanoparticles have shown excellent physicochemical characteristics and increase the transport of loaded compounds into cells and the retention of these compounds intracellularly thereby greatly increasing the anticancer effects in vitro against MCF-7 cancer cells than compounds without nanoparticles (Mosquera *et al.*, 2018; Pochapski *et al.*, 2021).

A central mechanism by which efficacious anti-cancer activity works is through inducing apoptosis at the molecular level. The caspase genes are the major regulator of the internal pathway of apoptosis, in which they participate.in activating executioner caspases, which ultimately leads to programmed cell death (Li *et al.*, 2017). Apoptosis-related gene expression studies using RT-qPCR provide an addition to cytotoxicity studies, allowing for insight into how cytotoxicity occurs via mechanisms involved with apoptosis (Livak and Schmittgen, 2001; Nolan *et al.*, 2006).

The evaluation of cytotoxicity in normal cells is significant in determining the specificity of possible anticancer nanomaterials. According to this study, Eugenol-AgNPs made from Eugenol-rich compound obtained from Fagonia indica, has shown potential cytotoxic effectiveness against MCF-7/C3 breast cancer cells.

This study evaluates anticancer activity of Eugenol-rich fraction obtained from Fagonia indica, through phytochemical identification, chromatography of the extract, and made silver nanoparticles to create a nanomedicine that can be used to determine cytotoxicity, and expression of genes involved in apoptosis in MCF-7 breast cancer cell lines.

2. MATERIALS AND METHODS

2.1 Plant Material and Extraction

The aerial part of Fagonia indica plant (Shokaa) were collected from Al-Shabaka region from Najaf governorate of Iraq, rinsed with water and dried by air. After which they were finely milled into powders and stored in sterile containers until needed.

22. Extraction and GC-MS Analysis

The extraction steps were carried out by soaking to extract the active compounds according to the method described by Harborn (1998). 100 grams of ground aerial parts of *Fagonia indica* were weighed, and the powder was soaked in 1 liter of 70% (v/v) ethanol at a ratio of 1:10 w/v for 72 hours with continuous stirring on a shaker at 150 rpm at room temperature. Gas chromatography–mass spectrometry (GC–MS) was employed for the analysis of the alcoholic extract. A separation was done by using DB-5MS capillary column (30 m × 0.25 mm i.d., 0.25 μm film thickness) using helium gas (≥99.999% purity) as carrier gas at a constant flow rate of 1.0 mL/min. The oven temperature was set at 60°C and kept for 2 minutes before slowly being ramped up to 280°C at a rate of 5°C per minute. This temperature was maintained for a duration of 10 minutes. The injector temperature was set at 250°C, and the sample was injected using a split ratio of 1:20. Electron ionization (EI) mass spectrometry with a voltage of 70 eV was used for the detection, with a scanning range of m/z 40-500. The mass spectra were compared to the mass spectra obtained from the NIST mass spectrometry database. Eugenol was preliminarily identified via GC-MS by means of its retention time, and by matching it with the mass spectral library data. The identification was later confirmed using HPLC-DAD against the authentic Eugenol standard as well as through the standard addition method.

2.3 Eugenol Enrichment and fraction collection by analytical HPLC

Through high-performance liquid chromatography, Eugenol was enriched from an alcoholic extract.. Before HPLC fractionation, crude extract were dissolved in methanol to achieve a concentration of 10 mg/mL. Given a volume of injection equal to 20 μL for the HPLC run. For this particular case, the crude extract was dissolved in methanol reaching a final concentration of 1 mg/mL, then filtered prior to HPLC injection. The HPLC run total time was equal to 30 minutes. The HPLC system was fitted with a ZORBAX Eclipse XDB-C18 analytical reversed-phase column (250 × 4.6 mm, 5 μm; Agilent Technologies, USA) and functioned under isocratic conditions using a methanol-water mobile phase (60:40, v /v). An injection volume of 20 microliters was used for each chromatographic operation. and subsequently confirmed by HPLC-DAD. Fractions were gathered on the basis of the retention time of Eugenol identified originally using the GC-MS technique followed by verification with HPLC-DAD technique. The chromatographic fraction corresponding to eugenol peak was collected from the retention time window from 7.8- 8.2 mins. The chromatographic separation and the process of collection were performed for 50 different injections, with a mass of the crude extract up to 10 mg. The fractions obtained after each collection contained Eugenol and were combined together. The collected fractions went through concentration under reduced pressure by means of a rotary evaporator in order to extract the solvent from the organic materials. The Eugenol-enriched portions were dried to a fixed weight and measured before proceeding to any additional investigation and the production of the nanoparticles. Fractions that contained the most significant concentration of Eugenol were re-injected by HPLC-DAD to determine their purity and concentration prior to developing nano-formulations for biological studies. The chromatographic fraction collection procedure was based on procedures stated by Yun et al (2010) and is commonly used for the enrichment of bioactive small molecules from complex plant samples. When it was time to load the nanoparticles, the eugenol-rich was dissolved again in aqueous alcohol at the required concentration.

2.4 Synthesis of Eugenol–AgNPs

Eugenol-AgNPs were prepared through a controlled chemical reduction method. First AgNO3 solution (1mM) in water was converted to colloidal Ag by adding freshly made NaBH4 (2mM) in solution under continuous stirring at room temperature. The formation of stable and uniform size of AgNP was shown by a change in color of the reaction mixture from clear to yellowish brown. The isolated Eugenol was mixed with suspension of the AgNP and stirred to allow for surface loading. The final product was collected from the mixture and used for physicochemical characterization and biological evaluation.

This method was chosen due to its simplicity, reproducibility, and production of stable, uniformly distributed AgNPs for potential biomedical use (Nocerino *et al.*, 2024).

2.4.1 Assessment of Eugenol Loading Efficacy

To determine the amount of Eugenol entrapped onto the AgNPs, we measured the concentration of unbound Eugenol present in the supernatant after the completion of the loading process. The Eugenol encapsulated AgNPs were separated after incubation using centrifugation, and the supernatant was isolated for HPLC-DAD analysis. The concentration of unbound Eugenol was determined using the previously established Eugenol calibration curve. The amount of Eugenol loaded onto the AgNPs was calculated as the difference between the initial amount of Eugenol added and the amount remaining in the supernatant. Loading efficiency (LE%) was calculated according to the following equation: $LE(\%)=M_{initial}-M_{free} \setminus M_{initial} \times 100$

Under the experimental conditions employed, a loading efficiency of nearly 81% was achieved; thus suggesting that almost 81% of the Eugenol added initially was bound to the surface of the AgNPs while 19% was left unbound in the supernatant.

2.5 Nano-characterization

2.5.1.1 Fourier Transform Infrared Spectroscopy

Fourier Transform Infrared Spectroscopy (FTIR) was utilized to assess the functional groups contained within both free Eugenol as well as Eugenol-AgNPs. An FTIR device with an attenuated total reflectance (ATR) module was used to record the spectra. Spectra were recorded in the spectral range of 4000–400 cm^{-1}, with a spectral separation of 4 cm^{-1}, and an average of 32 scans per sample to ensure optimal signal-to-noise ratio. Without any further chemical treatments, samples were prepared as dry powders and directly deposited onto the ATR crystal (Stuart, 2004). The baseline corrections and instrument calibrations were done by using a standard reference sample prior to the measurements. All spectra were recorded at room temperature.

2.5.1.2 UV-Visible Spectroscopy Measurement Conditions

The electronic spectra of free Eugenol, silver nanoparticles (AgNPs), and Eugenol-AgNPs were recorded using a dual-beam UV-Vis spectrometer. Measurements were performed in the 200–800 nm spectral range using a quartz cell with a 1 cm optical path length. A neutralization blank for the background was created using either distilled water or an appropriate solvent (Skoog *et al.*, 2014).

The samples were diluted sufficiently to meet the criteria of no saturation of the absorption in the instrument's linear range. All measurements occurred at ambient temperature and the maximum λ value was documented for each sample..

2.5.1.3 TEM analysis

The morphology and structural features of the EugenolAgNPs were examined by transmission electron microscopy (TEM). A diluted nanosuspension was deposited onto carbon-coated copper grids and air-dried at room temperature. TEM and high-resolution TEM (HRTEM) images were acquired at an accelerating voltage of 200 kV to evaluate particle shape, size distribution, and crystallinity. Particle sizes were determined by analyzing more than 100 nanoparticles using ImageJ software, and results are expressed as mean ± SD (Williams and Carter, 2009).

2.6 Cell culture

In the current research, MCF-7/c3 human breast cancer cells, were obtained from the Al-Amin Center for Advanced Biotechnology, Iraq. It is derived from a positive Caspase-3 and contains a stable expression of human procaspase-3, was used (Yang *et al.*, 2001). The cell line was grown in DMEM supplemented with 10 % fetal bovine serum (FBS) and antibiotics, followed by incubation cultured under standard conditions (37 °C and 5 % CO_2).

2.7 MTT Assay

The cytotoxic activity of the EugenolAgNPs was evaluated in human MCF-7 breast cancer cells using the MTT assay. Through the dissolution of the compound with DMSO, a stock solution was created and then a series of dilutions were created between 0.125 and 50 μg/ml, while maintaining the final concentration of DMSO does not exceed 0.15% (v/v). Doxorubicin (5 μM) was used as a positive control. MCF-7 cells were treated with DMEM containing (10%) FBS and antibiotics and cultured for 24 hours at a density of (8X103) cells per well in 96-well plates. Once the cells had adhered to the surface, they were treated

with the specified concentrations of dilutions for 24 hrs. The MTT assay was employed to measure cell viability and the absorbance was measured at 570 nm. The levels of cell viability were expressed in relation to the control treatment made with vehicle only, and IC_{50} values were calculated from dose–response curves (Mosmann (1983).

2.8 Gene Expression Analysis by RT-qPCR

The relative mRNA expression of apoptotic-related genes in the MCF-7/C3 cells was measured using the RT-qPCR method after treating those cells with both Free Eugenol and Eugenol-AgNPs. The cells were treated with Free Eugenol using its corresponding IC_{50} and with Eugenol-AgNPs of 1.85 µg/mL for 24 hours. Total RNA was extracted utilizing the RNeasy Mini Kit (Qiagen, Germany) based on the protocol as described by the supplier. The concentration and purity of RNA were determined using the NanoDrop spectrophotometer. Only RNA samples that had an A260/A280 ranging from 1.8 to 2.0 and an A260/A230 ≥1.8 were used for subsequent assays. The quality of RNA was assessed by determining RNA Integrity Number (RIN), and only those samples that had RIN of ≥7 were used for cDNA synthesis. 1 µg of RNA was reverse-transcribed into cDNA using the High-Capacity cDNA Reverse Transcription Kit (Applied Biosystems, USA) following the instructions provided by the manufacturer. RT-qPCR was carried out using PowerUp SYBR Green Master Mix (Applied Biosystems, USA) on the Applied Biosystems QuantStudio 5 Real-Time PCR System. The reaction volume of 20 µL consisted of 10 µL of 2× SYBR Green Master Mix, 0.4 µL of each primer from the 10 µM stock solution, corresponding to 0.2 µM concentration for each primer, 2 µL of cDNA template, and each reaction was brought to the final volume with the addition of nuclease-free water. The amplification process included an initial denaturation phase of 95°C (10 minutes), followed by 40 amplification cycles, each with a denaturation step at 95°C (15 seconds) and at 60°C (30 seconds) for the annealing and extension reaction.

GAPDH was used as the reference gene for normalization. Each reaction was performed in triplicate, and three independent biological replicates were analyzed. Relative mRNA expression was calculated using the $2^{-}\Delta\Delta Ct$ method, with the untreated control group used as the calibrator. Data are presented as mean ± SD, and assessed for statistical significance by employing one-way ANOVA followed by Tukey's test (Livak and Schmittgen, 2001; Rao *et al.*, 2013). The sequences of the primers utilized are provided in Table 1.

Table 1. Primer sequences used for quantitative real-time PCR (RT-qPCR)

Gene	Primer sequence (5' → 3')
Caspase-3	F: GCA GCA GAA TTC AGT TCT GC R: GTA CAT AGC GAC TCG ATG
Caspase-8	F: CTG CTG AAG GTTCGTA GAA TC R: TCA GCA GTT GTC CAT TAC GT
Caspase-9	F: GAT CTT CTG CTG TTG CAT GA R: GCA GAC GCA TAC TTC TTA AT
GAPDH	F: GTA GGT GAA GCT CGA AGT R: GTA GAT GGT GAT GTG ATA TC

2.9 Calibration of Eugenol by HPLC-DAD

An Eugenol solution of standard concentration was created. Next, solutions with different concentration levels of 5, 10, 20, 40, 80, and 100 µg/mL were prepared. The analysis was performed using an HPLC-DAD instrument with a C18 column, with a methanol-water mixture as the mobile phase and a flow rate of 1.0 mL/min, at a detection depth of 280 nm. The standard solutions were injected, and the peak area for each concentration was recorded. A titration curve was then constructed by relating the peak area to the Eugenol concentration, and the linear regression equation and coefficient of determination (R^2) were calculated according to a published method for Eugenol analysis by HPLC (Yun *et al.*, 2010).

2.10 Eugenol Identification Using HPLC-DAD

The identity of Eugenol in Fagonia indica extract and the Eugenol component was verified through the process of chromatography using high-performance liquid chromatography (HPLC), a methanol-water mobile phase, an isocratic system, and a flow rate of 1.0 mL/min, with detection at 280 nm, based on a published method for Eugenol analysis by HPLC (Yun et al., 2010). Eugenol standard solutions at concentrations of 5–100 μg/mL were prepared to construct a calibration curve, and the peak areas were recorded at 280 nm. To confirm the identity, the retention time of Eugenol in the extract and the Eugenol-rich fraction was compared with that of the standard, and a standard addition (spiking) test was performed on the Eugenol-rich fraction and reanalyzed under the same chromatographic conditions. Measurements were taken three times, and results are expressed as mean ± standard deviation. Statistical differences between groups were analyzed using one-way ANOVA, followed by Tukey's post hoc test.

2.11 Chromatographic purity of the Eugenol-rich fraction

The chromatographic purity of the Eugenol-rich fraction was assessed using HPLC-DAD at 280 nm by comparing the retention time and Eugenol peak area with the standard material. The percentage of Eugenol peak area was calculated by area normalization, and the percentage in the crude extract was compared with that of the fraction after enrichment. The collected fraction was also re-injected to verify the stability and chromatographic purity of the Eugenol peak (Yun *et al.*, 2010).

2.12 Hydrodynamic Volume and Zeta Potential Measurement

The hydrodynamic volume and size distribution of Eugenol–AgNPss were evaluated according to standard principles of dynamic light scattering (DLS) nanoparticle analysis using a Malvern Zetasizer Nano ZS/ZEN3600. Samples were prepared in deionized water at a 1:10 dilution ratio, and measurements were performed at 25 °C, with the average particle size and PDI being recorded. The zeta potential was also measured using electrophoretic mobility under the same conditions. Measurements were performed in triplicate, and results were expressed as mean ± standard deviation (ISO 22412:2025; Bhattacharjee, 2016).

2.13 Crystallographic analysis of nanomaterials using XRD

X-ray diffraction (XRD) was used to analyze the crystal structure of the Eugenol–AgNPs. The diffraction pattern was recorded, the peak positions were determined at (2/theta) values, and the interfacial spacings (d-spacing) were calculated using Bragg's law. The crystal planes and Miller indices (hkl) were determined by comparing the experimental peaks with the standard reflectances of face-centered cubic (fcc) silver, according to the methodologies for characterizing crystalline nanomaterials (Cullity & Stock, 2001). The analysis was performed on the dried nanosample, and the crystal values used to characterize the silver phase were recorded.

2.14 Elemental Analysis of Eugenol–Ag Compound Using EDX

The elemental composition of Eugenol–AgNPs was determined using energy-dispersive X-ray spectroscopy (EDX) coupled with electron microscopy. The resulting spectrum was analyzed to identify the elements present and estimate their weight and atomic percentages, with the characteristic signals of silver, carbon, and oxygen being used to determine the elemental composition of the compound. The analysis was performed on the nanosample after preparation for microscopy, and the results were expressed as weight and atomic percentages.

2.15 Apoptosis Analysis Using Annexin V-FITC/PI and Flow Cytometry

Apoptosis in MCF-7/C3 cells was assessed using the Annexin V-FITC/PI assay followed by flow cytometry analysis. Cells were treated with free Eugenol extract, silver nanoparticles (AgNPs), and Eugenol–AgNPs, with 0.15% DMSO used as a control. After treatment, cells were stained with Annexin V-FITC and propidium iodide (PI), MCF-7/C3 cells were treated with Free Eugenol (1.0 mM), AgNPs (10 μg/mL), or a combination of Eugenol–AgNPs (1.85 μg/mL) for 24 h before performing Annexin V-FITC/PI staining. These concentrations were chosen to compare treatment-induced changes in apoptotic cell populations under the experimental conditions. Cells treated with 0.15% dimethyl sulfoxide (DMSO) served as the control group. Then flow cytometry was performed to determine the percentage of viable cells, early apoptosis, late apoptosis, and necrosis cell. The study was conducted with three separate biological replicates (n = 3), and the findings were presented as mean ± SD. Statistical comparisons among groups were done through one-way ANOVA after which Tukey's post

hoc test was performed, with p-value below 0.05 being regarded as statistically significant. The assay was performed according to the published principle of using Annexin V/PI to differentiate between cell death states (Vermes *et al.*, 1995).

2.16 Cytotoxicity and Selectivity towards Normal MCF-10A Cells

The cytotoxicity of free Eugenol and the Eugenol-AgNPs against normal MCF-10A cells was assessed using the MTT assay under the same experimental conditions used to evaluate toxicity against MCF-7/C3 cells. IC_{50} values were calculated from dose-response curves using nonlinear regression. The selectivity index (SI) of the nanocomposite was calculated by dividing the IC_{50} value in MCF-10A cells by the corresponding IC_{50} value in MCF-7/C3 cells, following the methodology used to evaluate the cytotoxicity of anticancer compounds (Mosmann, 1983).

2.17 Statistical Analysis

In triplicate (n = 3), all of the experiments were conducted, and the data was expressed as an average ± SD. In addition, appropriate post-hoc tests were used after conducting one-way ANOVA for statistical comparisons and significance was set at $p < 0.05$ (Motulsky, 2014).

3. RESULTS

3.1. GC–MS analysis of the alcoholic extract

The gas chromatography-mass spectrometry analysis (GC-MS) of the *Fagonia indica* extract revealed the presence of 48 compounds in varying relative proportions, some of which are listed in Table 2 including polar and nonpolar compounds, with retention times ranging from 7.957 to 25.132 minutes. Among the compounds that were detected eugenol (4-allyl-2-methoxyphenol) stood out as the abundant. It made up 26.45% of the relative peak area in the analysis.

Table 2: Selected putatively identified compounds detected in *Fagonia indica* extract by GC-MS

RT (min)	Compound	Relative area (%)	Library match score	CAS No.
7.957	4-allyl-2-methoxyphenol	26.45	99	97-53-0
8.853	Oxime, methoxy-phenyl-	2.03	87	1000222-86-6
16.022	MethylEugenol	6.52	98	93-15-2
16.673	Cycloisolongifolene, 8,9-dehydro-	0.35	83	1000151-28-0
17.352	Phenol, 2,5-bis(1,1-dimethylethyl)-	0.36	90	5875-45-6
17.712	2(4H)-Benzofuranone, 5,6,7,7a-tetrahydro-4,4,7a-trimethyl-, (R)-	0.51	91	17092-92-1
18.201	1H-Cycloprop[e]azulen-7-ol, decahydro-1,1,7-trimethyl-4-methylene-	0.95	99	6750-60-3
22.206	Dibutyl phthalate	2.66	94	84-74-2
22.417	Hexadecanoic acid, ethyl ester	1.40	99	628-97-7
23.543	Phytol	7.33	99	150-86-7
24.046	9,12,15-Octadecatrienoic acid, ethyl ester, (Z,Z,Z)-	0.71	99	1191-41-9
25.132	9-Octadecenoic acid, 12-hydroxy-, methyl ester, [R-(Z)]-	1.47	91	141-24-2

Natural Resources for Human Health
eISSN: 2583-1194

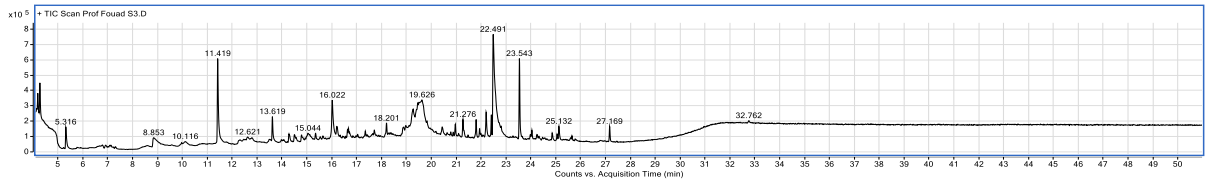

Fig. 1. GC–MS chromatogram of the ethanolic *Fagonia indica* extract

3.2. HPLC isolation and enrichment of Eugenol

The HPLC-DAD chromatogram of the Fagonia indica extract showed several chromatographic peaks (Fig. 2; Table 3). Among these, the peak representing 4-allyl-2-methoxyphenol, commonly known as Eugenol and had the highest relative peak area of 26.6% arrived at a retention time of 8.04 minutes. The identity of eugenol was confirmed using an original reference standard and a standard addition method. The final chemical identities of the remaining chromatographic peaks could not be determined because they were not confirmed using the original HPLC standards.

The other unidentified peaks collectively constituted 49.93% of the total chromatographic area, reflecting the chemical complexity of the crude extract.

Table 3. HPLC DAD chromatographic profile of the *Fagonia indica* extract

Peak No.	Assignment	RT (min)	Peak Area	Relative Area (%)
1	Chromatographic peak 1	4.23	316,000	2.06
2	Eugenol (confirmed using authentic standard andition)	8.04	4,080,000	26.6
3	Chromatographic peak 3	11.36	1,015,000	6.62
4	Chromatographic peak 4	14.63	147,000	0.97
5	Chromatographic peak 5	17.98	1,146,000	7.46
6	Chromatographic peak 6	19.36	422,000	2.75
7	Chromatographic peak 7	21.59	216,000	1.41
8	Chromatographic peak 8	23.09	108,000	0.72
9	Chromatographic peak 9	23.86	226,000	1.48
--	Other unassigned peaks (combined)	—	≈7,650,000	49.93

Natural Resources for Human Health
eISSN: 2583-1194

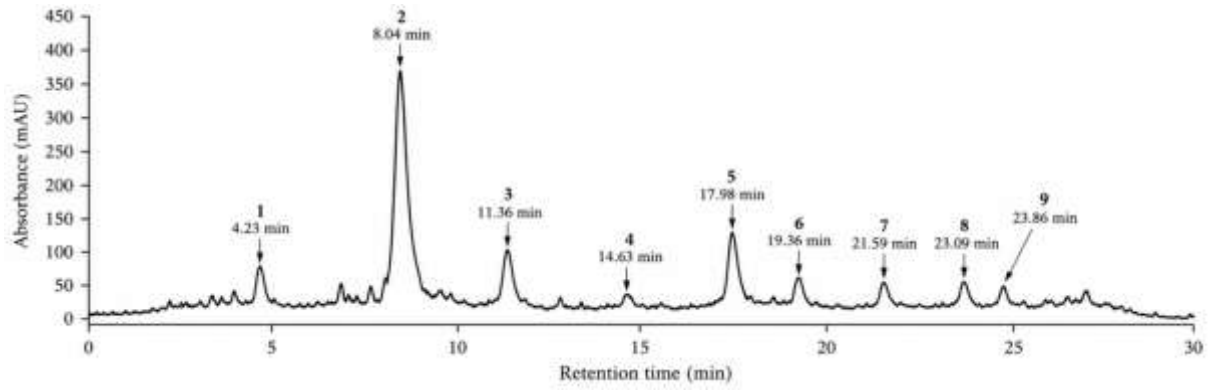

Fig. 2. HPLC-DAD chromatographic profile of the *Fagonia indica* alcoholic extract recorded at 280 nm

3.3 Characterization of EugenolAgNPs

3.3.1 FTIR Analysis

The results of table 4 of the FTIR analysis reveals spectral differences between the Eugenol compound in its free state and its silver-loaded state, confirming a genuine interaction between the compound and the nanoparticle surface (Table 4). The Eugenol-enriched fraction and the Eugenol-AgNPs exhibited various changes in spectral composition as determined by FTIR analysis (Table 4). The wide O–H stretching band showed a shift from 3434 to 3416 cm^{-1} along with reduction of intensity and broadening, implying alteration in the vicinity of hydroxyl groups after association with the surface of AgNP. Also seen were slight changes to the aromatic C=C, C–H bending, CH_3/CH bending, and C–O stretching bands. Among these changes was a move in the position of the C–O band which shifted from 1239 cm^{-1} to 1254 cm^{-1} thus suggesting the likely participation of the oxygen-containing groups in the interactions with the nanoparticle surface. Moreover, the formation of a minor band at around 520–540 cm^{-1} could correspond to surface interactions of Ag–O type. Two bands detected at 1710 and 1694 cm^{-1} have not been described and could be unrelated to the presence of Eugenol. The spectral changes observed in this investigation support the assertion that the molecular environment has changed due to the interaction of the Eugenol-enriched fraction with the AgNPs.

Table 4. FTIR spectral comparison of the Eugenol-enriched fraction and Eugenol–AgNPs

Wavenumber–Eugenol - enriched fraction (cm^{-1})	Wavenumber–Eugenol- Ag (cm^{-1})	Proposed assignment	Interpretation
3434 (broad)	3416 (broader, reduced intensity)	O–H stretching (Phenolic hydroxyl)	Decreased intensity and widened peak = interaction of hydroxyl groups with the AgNPs surface
1710 (sharp)	1694	Unassigned band	The observed shift in the suggests a change in the local chemical environment following interaction with the silver nanoparticle surface
1610	1625	Aromatic C=C stretching	A slight change in frequency results from the interaction of the π-electron system with the particle surface.
1444	1456	C–H bending (aromatic/aliphatic)	The change in intensity reflects a different chemical environment after nano-loading

Wavenumber–Eugenol - enriched fraction (cm^{-1})	Wavenumber–Eugenol- Ag (cm^{-1})	Proposed assignment	Interpretation
1370	1382	CH_3/CH bending vibrations	Evidence of a non-covalent association between Eugenol and silver
1239	1254	C–O stretching	The shift of the peak supports the role of C–O groups in the stabilization process.
—	520–540 (weak band)	Ag–O-related surface interaction	The emergence of a weak band in this region may be associated with interactions involving the silver nanoparticle surface.

3.3.2 UV–Vis Spectral Analysis

Table 5 lists the UV-Vis spectroscopy results for the optical characteristics of the free Eugenol and the Eugenol-silver nanocomposite. As illustrated, free Eugenol displayed a typical absorption peak at λmax ≈ 272 nm, which is due to π–π transitions linked to the molcular aromatic system and confirms the preservation of the compound's electronic structure. Unlike Eugenol, the silver nanoparticles displayed an absorption peak of approximately 417 nm, which is typical for surface plasmon resonance (SPR) and verifies the presence of silver nanoparticles.

Upon loading Eugenol onto the surface of the silver nanoparticles, a shift of the SPR peak to a longer wavelength (≈ 432 nm) was observed with increasing spectral bandwidth, indicating the interaction of Eugenol with the nanoparticle surface and a change in the surrounding dielectric environment. Furthermore, the nanocomposite's retention of a π–π* peak at ≈ 275 nm, with some expansion, indicates that the Eugenol molecular structure remains intact without chemical decomposition during the nan loading process.

Table 5. UV–Vis Spectral Characteristics of Free Eugenol and EugenolAgNPs

Sample	λmax (nm)	Spectral feature	Interpretation
Free Eugenol	272 ± 3	π–π* transition (aromatic system)	The distinctive absorption of free Eugenol
Silver nanoparticles (AgNPs)	417 ± 4	Surface Plasmon Resonance (SPR)	Evidence of the formation of silver nanoparticles
Eugenol–AgNPs	432 ± 2	Red-shifted SPR band	Loading Eugenol onto the surface of AgNPs
Eugenol–AgNPs	275 ± 1	Retained π–π* band (broadened)	Maintaining molecular structure with nano-interaction
Eugenol–AgNPs	—	Band broadening	Homogeneous size distribution and stable surface interactions

3.4 TEM Analysis

The results of the transmission electron microscopy analysis showed the morphological and structural properties of the Eugenol-AgNPs (Table 6 and Fig. 2). Low-magnification TEM images (Fig. 2a) show a homogeneous distribution of spherical

to spherical nanoparticles with minimal agglomeration, reflecting the good structural stability of the nanosystem. The metallic core size range is 35–55 nm with an average of 44.1 ± 6.7 nm, as shown in (table 6). This is smaller than the hydrodynamic diameter measured by DLS due to the absence of a hydrosphere and an organic layer in the TEM measurements.

High-resolution HRTEM images (Fig. 2 b–d) reveal distinct, periodic lattice lines, attributed to the (111) crystalline plane of face-centered cubic (fcc) silver. This also affirms the nanoparticles' high degree of crystallinity and that well-crystalline silver cores have formed. A thin organic layer around the particles can also be seen and is likely due to coating of the silver surface with Eugenol particles.

Table 6. TEM-Derived Morphological Characteristics of EugenolAgNPs

Parameter	Observation	Interpretation
Particle shape	Spherical to quasi-spherical	Regular spherical morphology consistent with the observed nanoscale structure
Core size range (nm)	35–55 nm	The actual size of the AgNPs nucleus
Mean particle size (nm)	44.1 ± 6.7	Smaller than DLS
Size distribution	Narrow, monomodal	Compliant with low PDI (0.22)
Agglomeration	Minimal	Good structural stability
Surface appearance	Organic coating visible	Eugenol layer on the surface of silver

The values are derived from the analysis of more than 100 nanoparticles using Image] software, and are represented as mean ± standard deviation.

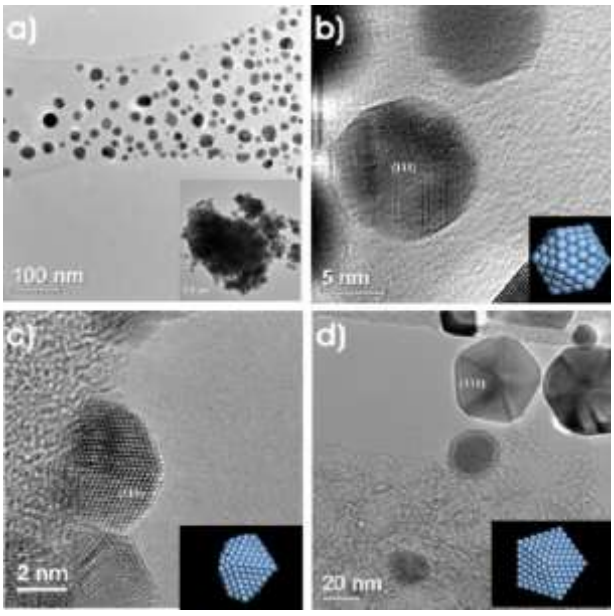

Fig. 2. TEM and HRTEM images of the EugenolAgNPs.

(a) Low-magnification TEM image showing uniformly distributed spherical to quasi-spherical nanoparticles.

(b,c) High-resolution TEM images revealing clear lattice fringes corresponding to the (111) crystallographic plane of face-centered cubic silver.

(d) TEM image showing faceted nanoparticles with good crystallinity and minimal aggregation.

3.5. Cytotoxic activity of EugenolAgNPs

MTT assays on human MCF-7/C3 breast cancer cells were used to evaluate cytotoxicity of Eugenol-AgNPs. By 24 hours after they received the composite, a clear dose-dependent decrease in cell viability was observed (Table 7, fig. 3). This also suggested

that there is a stepwise response for all dosages used in testing. Analysis of the dose–response relationship by nonlinear regression gives an IC_{50} value of 1.854 µg/ml, indicating potent in vitro cytotoxic activity under the tested conditions against MCF-7/C3 cells (Fig. 3). The lower IC_{50} observed for the nanocomposite compared with previously reported free Eugenol values suggests enhanced cytotoxic potency; however, direct comparison requires parallel testing under identical experimental conditions. At higher concentrations used (10–50 µg/mL), the cell viability stayed at almost the same level of around 10–11%, showing that the cytotoxic response reached its lower asymptotic level under the tested conditions. The solvent (DMSO at a concentration of 0.15%) did not significantly affect cell viability, confirming the safety of the testing system. Doxorubicin (5 µM), used as a positive control and reduced cell viability to 52.16 ± 3.74% in the current study, which indicates that MCF-7/C3 cells are responsive to the well-known cytotoxic drug tested.

Table 7. Effect of the Eugenol-AgNPs on the viability of MCF-7/C3 cells

Concentration (µg/mL)	Cell viability (%)
50	10.78 ± 0.43
25	10.82 ± 0.42
10	10.19 ± 0.19
5	26.44 ± 3.21
1	75.52 ± 2.49
0.5	78.55 ± 5.40
0.25	81.14 ± 6.35
0.125	85.26 ± 2.37
DMSO (0.15%)	100.00 ± 1.82
Doxorubicin (5 µM)	52.16 ± 3.74

The values represent the mean ± standard deviation (Mean ± SD) of 3 independent replicates (n = 3).

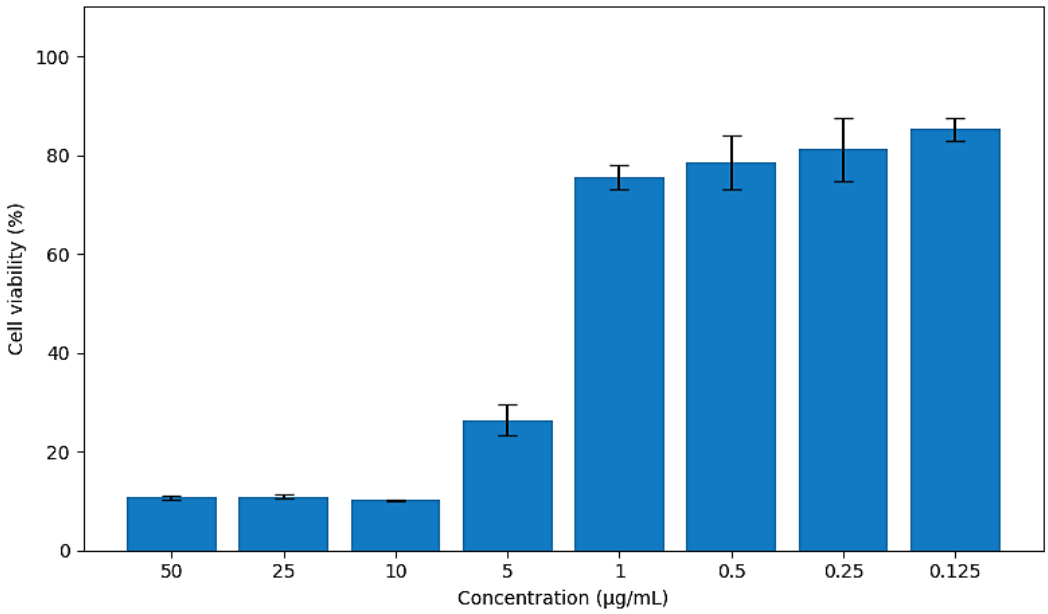

Fig. 3. Dose–response curve of EugenolAgNPs on MCF-7/C3 cells after 24 h treatment. Cell viability (%) was expressed relative to the DMSO-treated control (0.15%), which was set at 100%. Data are presented as mean ± SD of three independent experiments (n = 3).

Natural Resources for Human Health
eISSN: 2583-1194

3.6 Molecular Analysis of Gene Expression Associated with Apoptosis

Based on RT-qPCR data, the expression of genes associated with apoptosis is significantly higher in the MCF-7/C3 cell line after treatment with Eugenol–AgNPs and Free Eugenol (See Table 8 and Fig. 4). Eugenol–AgNPs exhibited stronger effects on the relative expression levels of Caspase-3 (2.42 ± 0.42-fold), Caspase-9 (2.09 ± 0.53-fold), and Caspase-8 (2.66 ± 0.34-fold) than Free Eugenol (1.59 ± 0.32-fold, 1.47 ± 0.29-fold, and 1.72 ± 0.38-fold) compared to control. The changes noted in mRNA expression confirm the involvement of apoptosis-associated signaling pathways and indicate an enhanced molecular response post treatment with Eugenol–AgNPs (Refer to Table 8; Refer to Fig. 4)

Table 8. The relative mRNA expressions of apoptosis-related genes in MCF-7/C3 cell line

Gene	Control (Fold Change)	Free Eugenol (Fold Change ± SD)	Eugenol-Ag nano (Fold Change ± SD)	p-value
Caspase-3	1.00	1.59±0.32	2.42±0.42	<0.001
Caspase-9	1.00	1.47±0.29	2.09 ±0.53	<0.001
Caspase-8	1.00	1.72±0.38	2.66 ±0.34	<0.01
GAPDH	References gene	References gene	References gene	>0.05 (ns)

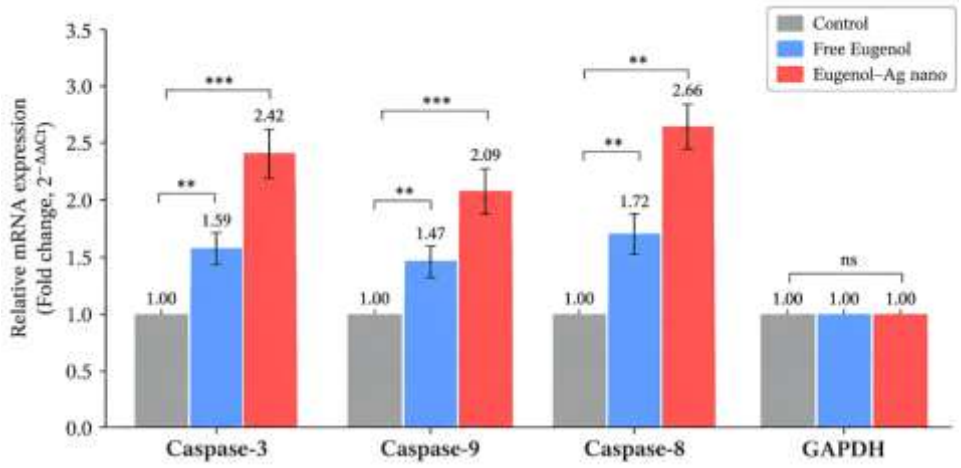

Fig. 4. Relative mRNA expression of apoptosis-related genes in MCF-7/C3 cells after treatment with free Eugenol and Eugenol-silver nanocomposite

3.7 HPLC-DAD Calibration of Eugenol

The standard titration curve for Eugenol in Table (9) showed a graded linear response within the concentration range of 5–100 µg/mL, with the peak area increasing from 113,430 at 5 µg/mL to 2,188,540 at 100 µg/mL. The titration data demonstrated an excellent linear relationship between concentration and peak area, according to the regression equation y = 21,833.52x + 3,305.32, with a coefficient of determination R^2 = 0.999997.

Table 9. Eugenol Standard Calibration Curve by HPLC-DAD

Eugenol standard (µg/mL)	Peak area
5	113,430
10	221,810

Eugenol standard (µg/mL)	Peak area
20	439,960
40	875,520
80	1,748,120
100	2,188,540

Regression: y = 21,833.52x + 3,305.32

R^2 = 0.999997

3.8 HPLC-DAD Retention Time Confirmation of Eugenol

The HPLC-DAD results for retention time confirmation showed a clear convergence among all samples (Table 10). The Eugenol standard had a retention time of 8.02 ± 0.04 minutes, while Fagonia indica extract recorded 7.99 ± 0.05 minutes, and the Eugenol-enriched fraction 8.01 ± 0.04 minutes. The standard addition (spiking) test also showed a time of 8.02 ± 0.04 minutes, consistent with the standard.

Table 10. Retention Time Confirmation of Eugenol by HPLC-DAD

Sample	Eugenol RT (min)
Eugenol standard	8.02 ± 0.04
Fagonia indica extract	7.99 ± 0.05
Eugenol-enriched fraction	8.01 ± 0.04
Spiked enriched fraction	8.02 ± 0.04

3.9 Chromatographic Purity of the Eugenol-Enriched Fraction

The chromatographic analysis summarized in Table (11) confirmed the successful enrichment of Eugenol from the crude alcoholic extract obtained from Fagonia indica. The relative peak area of Eugenol in the crude extract was 26.6%, while the chromatographic purity of the resultant Eugenol-enriched fraction reached 94.7 ± 1.5% by HPLC analysis.

Table 11. Chromatographic purity of the Eugenol-Enriched Fraction

Parameter	Result
Eugenol relative area in the crude extract	26.6%
Chromatographic purity of the enriched fraction	94.7 ± 1.5%

Natural Resources for Human Health
eISSN: 2583-1194

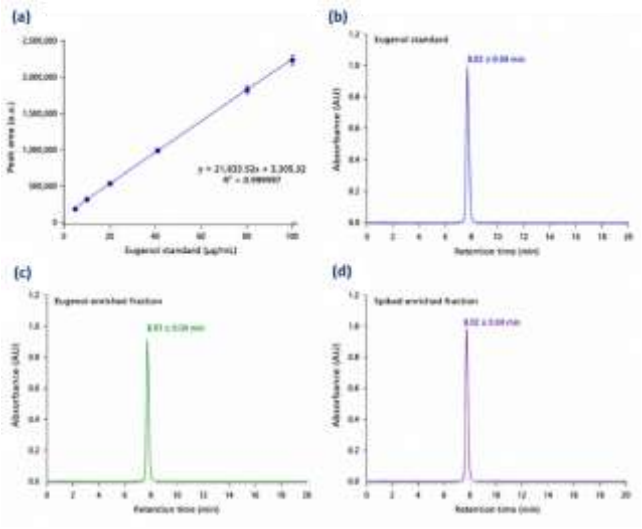

Fig. 5. HPLC-DAD. Confirmation of Eugenol: (a) calibration curve of Eugenol standards ranging from 5 to 100 µg/mL; (b) chromatogram of the Eugenol standard showing a clear peak; (c) chromatogram of the Eugenol-enriched fraction with a peak at around 8.0 minutes; (d) chromatogram of the spiked Eugenol-enriched fraction, where the peak appears at the same retention time as, in the standard confirming consistent results at approximately 8.0 minutes.

3.10 Characterization of the Hydrodynamic Size and Surface Potential of the Eugenol–AgNPs

The results of table 12 shows that the Dynamic Light Scattering (DLS) analysis data for the Eugenol–AgNPss revealed a mean hydrodynamic diameter of 68.6 ± 5.4 nm, with a PDI value of 0.219 ± 0.027, reflecting a relatively narrow particle size distribution. The zeta potential was −24.8 ± 2.9 mV.

Table 12. Dynamic Light Scattering and Zeta Potential Characteristics of the Eugenol–AgNPs

Parameter	Eugenol–AgNPs
Hydrodynamic diameter (DLS)	68.6 ± 5.4 nm
PDI	0.219 ± 0.027
Zeta potential	−24.8 ± 2.9 mV

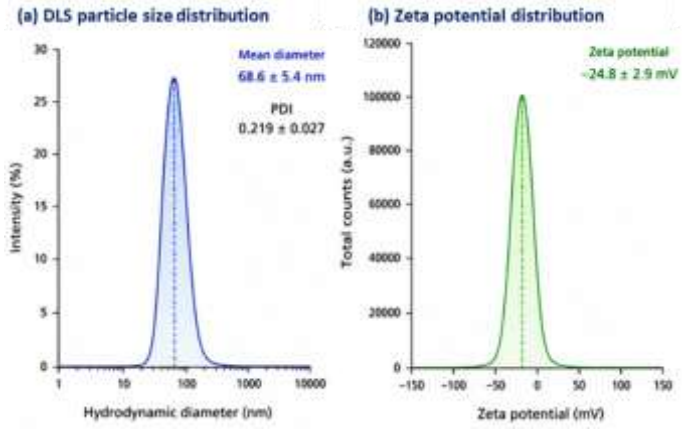

Fig. 6. DLS particle-size distribution (a), and zeta potential of the Eugenol–AgNPs (b)

Natural Resources for Human Health
eISSN: 2583-1194

3.11 Crystallographic Analysis of the Nanomaterial Using X-ray Diffraction (XRD)

The findings of X-ray diffraction techniques stated in the Table (13) display four principal peaks within the 2θ spectrum at the angles of 38.14°, 44.33°, 64.46°, and 77.42° corresponding to the crystal plan of (111), (200), (220), and (311) respectively, with d-spacing values of 2.358, 2.042, 1.446, and 1.232 Å. These reflections were attributed to face-centered cubic silver (fcc Ag).

Table 13. X-ray Diffraction Peaks and Crystallographic Parameters of the Eugenol–AgNPs

Assignment	Miller index (hkl)	d-spacing (Å)	2θ (°)
Ag, fcc	(111)	2.358	38.14
Ag, fcc	(200)	2.042	44.33
Ag, fcc	(220)	1.446	64.46
Ag, fcc	(311)	1.232	77.42

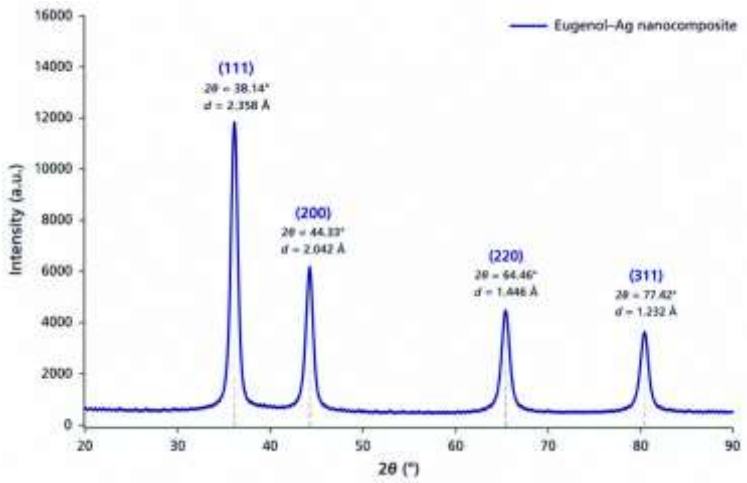

Fig. 7. X-ray diffraction pattern of the Eugenol–AgNPs showing the characteristic fcc Ag reflections

3.12 Elemental Analysis of the Eugenol–AgNPs Using EDX

The results of shows the results of the energy-dispersive X-ray spectroscopy (EDX) analysis(Table 14; Fig. 8), indicating that silver (Ag) is the highly concentrated element in the nanocomposite with its percentage values by weight of 88.6 and by atomic percentage of 65.3. The percentage weight of carbon (C) is 7.3, which is equivalent to 21.1 of the atomic percentage, while the percentage weight of oxygen (O) is 4.2, and by total atomic percentage is 13.7. EDX analysis characterized the elemental composition of the nanocomposite with Silver being the main component with C and O signals being detected the confirmation of Eugenol loading cannot be independently verified due to possible contribution from the background signals and the sample support. Hence, the evidence of Eugenol being associated with nanocomposite can only be established through the FTIR determination and quantitative HPLC analysis.

Table 14. EDX Elemental Composition of the Eugenol–AgNPs

Element	Weight (%)	Atomic (%)
Ag	88.6	65.3

Natural Resources for Human Health
eISSN: 2583-1194

Element	Weight (%)	Atomic (%)
C	7.3	21.1
O	4.2	13.7
Total	100.0	100.0

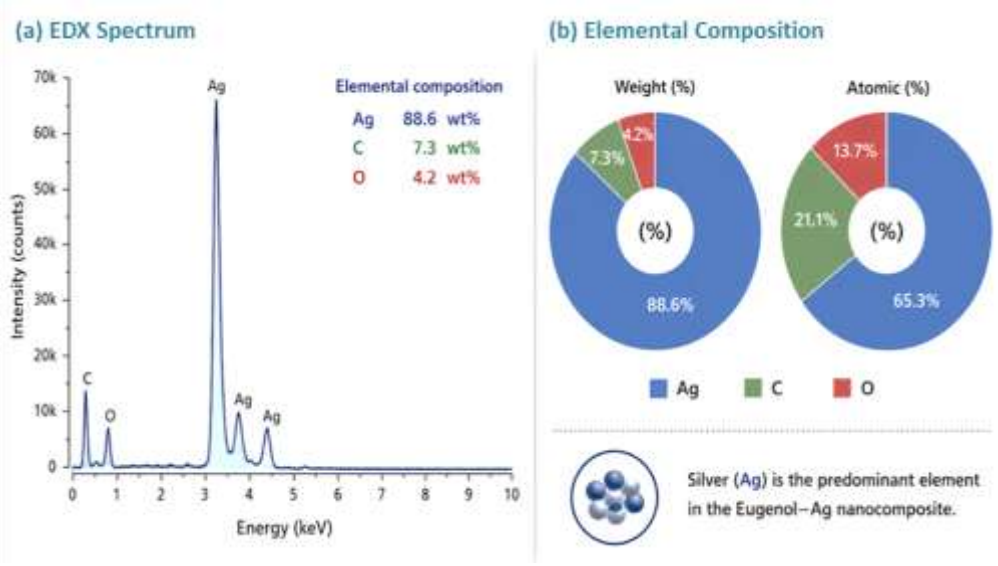

Fig. 8. EDX characterization of the Eugenol–AgNPs: (a) EDX spectrum showing the characteristic elemental signals of Ag, C, and O; and (b) corresponding elemental composition based on weight and atomic percentages

3.13 Apoptosis Analysis Using Annexin V-FITC/PI Flow Cytometry

Annexin V-FITC/PI analysis, as shown in Table 15, revealed a clear difference in the distribution of MCF-7/C3 cells between the treatment groups. The percentage of viable cells was 91.9 ± 0.51% in the control group, compared to 48.7 ± 0.69% with Eugenol and 56.5 ± 0.61% with AgNPs, and decreased to 19.8 ± 0.60% after treatment with the Eugenol-AgNPs. Early and late apoptosis rates were 25.9 ± 0.51% and 47.8 ± 0.09%, respectively, in the Eugenol-Ag group, compared to 19.8% and 24.9% with Eugenol and 16.3 ± 0.45% and 21.6% with AgNPs. Necrosis rates were 2.5 ± 0.25%, 6.6 ± 0.29, 5.6 ± 0.20%, and 6.5 ± 0.09% in the control, Eugenol, AgNPs, and Eugenol-Ag groups, respectively.

Table 15. Annexin V-FITC/PI Flow Cytometric Analysis of Apoptosis in MCF-7/C3 Cells Treated with Eugenol–AgNPs

Treatment	Viable (%)	Early apoptosis (%)	Late apoptosis (%)	Necrosis (%)
Control (DMSO 0.15%)	91.9 ± 0.51	3.3 ± 0.19	2.3 ± 0.19	2.5 ± 0.25
Free Eugenol	48.7 ± 0.69	19.8 ± 0.43	24.9 ± 0.35	6.6 ± 0.29
AgNPs	56.5 ± 0.61	16.3 ± 0.45	21.6 ± 0.26	5.6 ± 0.20
Eugenol–AgNPs	19.8 ± 0.60	25.9 ± 0.51	47.8 ± 0.09	6.5 ± 0.09

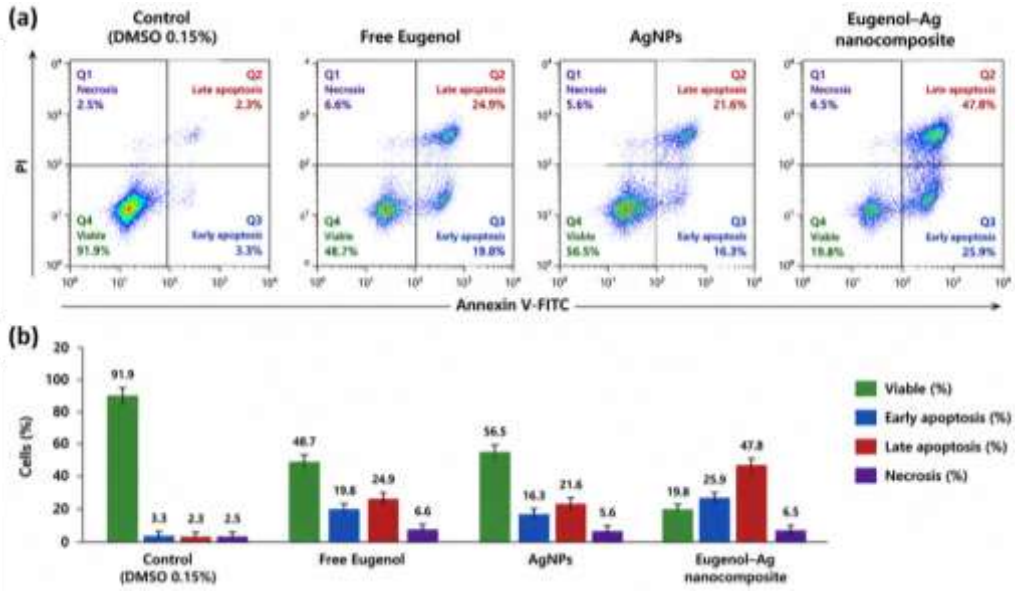

Fig. 9. Apoptosis detection via flow cytometric analysis using annexin V-FITC/PI of MCF-7/C3 cells which were treated with Eugenol, AgNPs and Eugenol–AgNPs. (a) The flow cytometric dot plots coinciding to the cell populations which are viable, in early apoptosis, in late apoptosis and necrotic cells. (b) The quantitative distribution of the respective cell populations.

3.14 Cytotoxicity and Selectivity towards Normal MCF-10A Cells

The results of the cytotoxicity test on MCF-10A cells, shown in Table (16), indicate that the IC_{50} value was 18.73 ± 1.37 µg/mL for Eugenol and 9.85 ± 0.83 µg/mL for the Eugenol-AgNPs. The selectivity index (SI) was 5.31, based on the IC_{50} value of the nanocomposite in MCF-7/C3 cells, which was 1.854 µg/mL.

Table 16. Cytotoxic Activity of Free Eugenol and Eugenol–AgNPs against MCF-10A Cells

Treatment	IC_{50} (µg/mL)
Free Eugenol	18.73 ± 1.37
Eugenol–AgNPs	9.85 ± 0.83

Selectivity index (SI)= 5.31

4. DISCUSSION

In the current work, the researchers adopted a sequential strategy with the objective of applying chemical profiling of Fagonia indica followed by chromatographic isolation of the Eugenol and its incorporation into a silver-containing nanosystem. Results achieved from the GC–MS profiling revealed Eugenol to be the main constituent of the extract, but since the library match was rather modest, its identification via GC–MS alone could only be considered tentative. The confirmation of retention times with an actual Eugenol standard and the HPLC-DAD's favorable spiked responses definitely offered a strong verification of the identity of the compound. The complementary analytical method is greatly applicable for complicated plant extracts, where they process the filing chromatography method to obtain the desired components and study the biological effects on them (Yun *et al.*, 2010; Queiroz *et al.*, 2024).

The chromatographic results comprehensively present a chemical rationale for moving forward with biological experiments based on the crude extract. The increase in the relative peak area of Eugenol, after the operation of fractionation of the crude extract, shows that Eugenol has been fractionated in a more concentrated way. Furthermore, the independent determination of the purity of the fraction that was collected proves that it has been sufficiently enriched for subsequent applications. This difference is significant as both relative peak area and chromatographic purity are not equivalent analytical parameters. The

utilization of HPLC in recovering Eugenol from a complex matrix is compatible with HPLC methods of measurement of Eugenol and more generally with various chromatographic methods used in the extraction of natural products (Said *et al.*, 2025; Al-Burki , 2026).

The physicochemical characterization leads to the conclusion for the formation of the Eugenol-AgNPs and supports an explanation of its *further* biological behavior. The FTIR shifts suggest changes in chemical environment of functional groups during loading, indicating interaction of Eugenol with silver surface while the UV-Vis red shift of surface plasmon band of silver provides supporting evidence of modification of interfacial environment of the nanoparticles. This kind of spectral alteration can be attributed to the impact of surface chemistry and surrounding dielectric environment on the optical properties of metallic nanoparticles (Coates, 2000; Kelly *et al.*, 2003). Features related to the spherical shape and fcc crystalline structure of silver nanoparticles that are visible through TEM/HRTEM and XRD examination correlate with the known traits of chemically synthesized silver nanoparticles (Sun and Xia, 2002; Nocerino *et al.*, 2024). The finding that the TEM shows a lower size than the DLS hydrodynamic diameter can be expected since DLS includes not only the particle itself but the surrounding solvated layer and other surface components (Bhattacharjee, 2016).

The biological analysis shows that the nanocomposite has significant in vitro cytotoxic effect on the MCF-7/C3 cells, as indicated by the profiling with Annexin V/PI, which suggests that the cell death is caused by apoptosis. This observation makes biological sense because previous reports refer to Eugenol as a phenolic compound able to inhibit the growth of cancer cells and activate apoptosis via mechanisms related to cellular stress and apoptosis (Jaganathan and Supriyanto, 2012; Ulanowska and Olas, 2021). Prior studies in breast cancer models have likewise linked Eugenol exposure with oxidative stress and disruption in mitochondrial functionality, but these processes were not specifically evaluated in the present investigation and should therefore not be assumed to be proven (Noman *et al.*, 2025). The significantly smaller IC_{50} for the nanocomposite suggests that nanoscale formulation may change the way the biological availability of the loaded compound or its interaction with cells occurs. Still, caution should be exercised here, as it would be inappropriate to directly compare it to free Eugenol.

Molecular evidence further supports the view of apoptosis. The rise in Caspase-3 expression suggests involvement of the execution phase of apoptosis, whereas the simultaneous increase in Caspase-8 and Caspase-9 points to the involvement of both extrinsic and intrinsic pathways. Caspase-9 is a crucial factor in the intrinsic apoptotic pathway; hence, the merging of initiator signals on the effector caspase follows the mechanistic approach underlying the apoptotic outcome observed in the Annexin V/PI test (Li *et al.*, 2017). The obtained data correspond with the previously published information dedicated to Eugenol-induced apoptosis (Jaganathan and Supriyanto, 2012; Ulanowska and Olas, 2021). In contrast, the RT-qPCR findings indicate that mRNA gene expression is altered rather than indicating activation of caspase and/or its enzymatic activity. Thus, the results indicate a possible role of the apoptotic pathways, but do not demonstrate sufficient evidence of involvement of either intrinsic or extrinsic pathways.

Ultimately, the higher IC_{50} value of the Eugenol–AgNPs in MCF-10A cells, when viewed against the same stain in MCF-7/C3 cells, yielded a selectivity index of 5.31, which indicates that there is a difference in sensitivity between the two cellular models. This first observation provides support to the biological importance of the cytotoxicity findings, as the effect was not exclusively tested in the cancer-cell model. Nonetheless, it is necessary to differentiate between the intracellular selectivity of cell lines and their application in clinical practice and tumor specificity. Overall, the chemical identity of Eugenol, combined with its separation via chromatography, the characterization of the Ag nanosystem, and confirmatory findings obtained from tests of cytotoxicity, apoptosis, and gene expression create a strong rationale for studying the Eugenol–Ag composite for anticancer research.

5. CONCLUSION

The fiding of this study demonstrate that Eugenol-AgNPs prepared using an Eugenol-rich fraction obtained from *Fagonia indica*, exhibited dose-dependent in vitro cytotoxic activity against MCF-7/C3 breast cancer cells, with an IC_{50} value of 1.854 μg/mL. The physicochemical properties were characterized using FTIR, UV–Vis, TEM/HRTEM, DLS, XRD, EDX, and zeta potential spectroscopy complemented the synthesis and characterization of Eugenol–AgNPs. Annexin V-FITC/PI assay revealed that treatment of Eugenol–AgNPs resulted in increased apoptotic population of cells. Moreover, results obtained from RT-qPCR analyses indicate that there was higher mRNA expression of the three apoptosis-related genes, namely, Caspase-3, Caspase-8, and Caspase-9. The findings suggest that there is a link between the cytotoxic impacts of Eugenol-AgNPs and the activation of

apoptotic processes, but it cannot be claimed that the findings demonstrate any activation of caspase enzymes or point out whether intrinsic or extrinsic apoptosis routes are involved. Eugenol–AgNPs were confirmed to have differential cytotoxicity against different cancer and non-cancer cell lines, with a selectivity index of 5.31. All of these findings indicate the promise of Eugenol–AgNPs as a candidate for further research on the treatment of breast cancer through in vitro and preclinical tests.

Funding
This research received no external funding.

Acknowledgement

The authors sincerely thank the Al-Amin Center for Advanced Biotechnology in Iraq for supplying the MCF-7/c3 cell line for the purpose of this study.

Author Contributions

Asseel Majeed Alamery: Investigation, formal analysis, and writing the manuscript.

Fouad Razzaq Al-Burki: Supervision of the study, methodology, interpretation of data, revising the manuscript critically.

Asia Ali Hamza: Data collection, and writing the manuscript.

Muder Al-Hayder: Conceptualization, methodology, writing the manuscript, and administration of the project.

All authors have reviewed and agreed for the final version of the manuscript.

Conflict of Interest

The authors declare that they do not have any financial or personal relationship influence their work in this manuscript.

Ethics Statement

The study included only well-established human cancer and non-cancer cell lines and did not involve participants or experimental animals. Therefore, ethical approval and informed consent are not required in this regard.

Data Availability

Supporting data for the conclusion of this study are available following reasonable request to the corresponding author..

REFERENCES

[1] Al-Burki, F.R. (2026). Plant Chemistry. Ministry of Higher Education and Scientific Research. Jaber Ibn Hayyan University of Medical and Pharmaceutical Sciences - Iraq. 451p.

[2] Ali, M. L., Noushin, F., Sadia, Q. A., Metu, A. F., Meem, J. N., Chowdhury, M. T., Azme, E. (2025). Spices and culinary herbs for the prevention and treatment of breast cancer: a comprehensive review with mechanistic insights. Cancer Pathogenesis and Therapy, 3(03), 197-214.

[3] Atanasov, A. G., Zotchev, S. B., Dirsch, V. M., & Supuran, C. T. (2021). Natural products in drug discovery: Advances and opportunities. Nature Reviews Drug Discovery, 20(3), 200–216. https://doi.org/10.1038/s41573-020-00114-z

[4] Bhattacharjee, S. (2016). DLS and zeta potential – What they are and what they are not? Journal of Controlled Release, 235, 337–351. https://doi.org/10.1016/j.jconrel.2016.06.017

[5] Celik, I., Cihangiroglu, M., Ilhan, N., Akpolat, N., & Akbulut, H. H. (2005). Protective effects of different antioxidants and Eugenol on vancomycin-induced nephrotoxicity. Basic & clinical pharmacology & toxicology, 97(5), 325-332.

[6] Celik, S., Akyuz, S., Ozel, A. E., & Akalin, E. (2023). Vibrational spectroscopic and molecular docking studies of Eugenol, a cardiotonic inotropic drug. Optics and Spectroscopy, 131(7), 489-503.

[7] Coates, J. (2000). Interpretation of Infrared Spectra, A Practical Approach. In R. A. Meyers (Ed.), Encyclopedia of Analytical Chemistry: Applications, Theory and Instrumentation, pp. 10815–10837. John Wiley & Sons. https://doi.org/10.1002/9780470027318.a5606

[8] Kuo, C. Y.; Yang, T. H.; Tsai, P. F.; Yu, C. H. Role of the inflammatory response of RAW 264.7 cells in the metastasis of novel cancer stem-like cells. Medicina 2021, 57 (8), 778 DOI: 10.3390/medicina57080778

[9] Cullity, B. D., Stock, S. R. (2001). Elements of X-ray diffraction (3rd ed.). Prentice Hall.

[10] Gurunathan, S., Han, J. W., Eppakayala, V., & Kim, J. H. (2014). Green synthesis of silver nanoparticles using plant extracts and their anticancer activity. International Journal of Nanomedicine, 9, 545–558. https://doi.org/10.2147/IJN.S51729
[11] Hago, S., Lu, T., Abdelgadir, A. A., Yassin, S., Ahmed, E. M., Xu, H. (2023). Phytochemical Constituents and In-Vitro Anticancer Activity of some Medicinal Plant Extracts against MCF-7 and MDA-MB-435 Human Breast Cancer Cell Lines. Tropical Journal of Natural Product Research. 7(3), 2506–2515. https://doi.org/10.26538/tjnpr/v7i3.6
[12] Harborne, J.B. (1998). Phytochemical Methods: A Guide to Modern Techniques of Plant Analysis. springer science & business media.
[13] Harvey, A.L., Edrada-Ebel, R.,Quinn, R.J. (2022). The re-emergence of natural products for drug discovery in the genomics era. Nature Reviews Drug Discovery, 21(1),1-17.
[14] Jaganathan, S.K., Supriyanto, E., (2012). Antiproliferative and molecular mechanism of Eugenol-induced apoptosis in cancer cells. Molecules, 17(6), 6290–6304.
[15] Kamatou, G. P., Vermaak, I., & Viljoen, A. M. (2012). Eugenol—from the remote Maluku Islands to the international market place: A review of a remarkable and versatile molecule. Molecules, 17(6), 6953–6981. https://doi.org/10.3390/molecules17066953
[16] Kelly, K. L., Coronado, E., Zhao, L. L., & Schatz, G. C. (2003). The optical properties of metal nanoparticles: The influence of size, shape, and dielectric environment. The Journal of Physical Chemistry B, 107(3), 668–677.
[17] Li, P., Zhou, L., Zhao, T., Liu, X., Zhang, P., Liu, Y., Zheng, X., Li, Q. (2017). Caspase-9: structure, mechanisms and clinical application. Oncotarget. 8(14): 23996–24008.
[18] Livak, K. J., Schmittgen, T. D. (2001). Analysis of relative gene expression data using real-time quantitative PCR and the $2^{-}\Delta\Delta Ct$ method. Methods, 25(4), 402–408.
[19] Mahmood, T., Yang, P.-C. (2012). Western blot: Technique, theory, and trouble shooting. North American Journal of Medical Sciences, 4(9), 429–434. https://doi.org/10.4103/1947-2714.100998
[20] Marchese, A.; Barbieri, R.; Coppo, E.; Orhan, I. E.; Daglia, M.; Nabavi, S. F.; Izadi, M.; Abdollahi, M.; Nabavi, S. M.; Ajami, M. Antimicrobial activity of Eugenol and essential oils containing Eugenol: A mechanistic viewpoint. Crit Rev. Microbiol. 2017, 43, 668– 689, DOI: 10.1080/1040841X.2017.1295225
[21] Meyers (Ed.), Encyclopedia of Analytical Chemistry (pp. 10815–10837). John Wiley & Sons.
[22] Mosmann, T. (1983). Rapid colorimetric assay for cellular growth and survival: Application to proliferation and cytotoxicity assays. Journal of Immunological Methods, 65(1–2), 55–63. https://doi.org/10.1016/0022-1759(83)90303-4
[23] Mosquera, J., García, I., Liz-Marzán, L. M. (2018). Cellular uptake of nanoparticles versus small molecules: A matter of size and surface chemistry. Accounts of Chemical Research, 51(9), 2305–2313.
[24] Motulsky, H. J. (2014). Intuitive Biostatistics: A Nonmathematical Guide to Statistical Thinking (3rd ed.). Oxford University Press, New York, USA.
[25] Murakami, Y.; Kawata, A.; Fujisawa, S. Expression of Cyclooxygenase-2, Nitric Oxide Synthase 2 and Heme Oxygenase-1 mRNA Induced by Bis-Eugenol in RAW264.7 Cells and their Antioxidant Activity Determined Using the Induction Period Method. In Vivo 2017, 5, 819– 831, DOI: 10.21873/invivo.11135
[26] Newman, D. J., & Cragg, G. M. (2020). Natural products as sources of new drugs over nearly four decades. Journal of Natural Products, 83(3), 770–803. https://doi.org/10.1021/acs.jnatprod.9b01285
[27] Nocerino, V., Miranda, B., Dardano, P., Sanità, G., Esposito, E., & De Stefano, L. (2024). Protocol for synthesis of spherical silver nanoparticles with stable optical properties and characterization by transmission electron microscopy. STAR protocols, 5(1), 102920.
[28] Nolan, T., Hands, R. E., & Bustin, S. A. (2006). Quantification of mRNA using real-time RT-PCR. Nature Protocols, 1(3), 1559–1582. https://doi.org/10.1038/nprot.2006.236
[29] Noman, A. M., Sultan, M. T., Mazhar, A., Khan, W. A., Imran, M., Hussain, M., & Al Abdulmonem, W. (2025). Eugenol: An Insight Into the Anticancer Perspective and Pharmacological Aspects. Food Science & Nutrition, 13(8), e70727.
[30] Pires Costa, E., Maciel dos Santos, M., de Paula, R. A., da Silva, D. A., Lopes, R. P., Teixeira, R. R., & Gonçalves, R. V. (2025). Antioxidant and anti-inflammatory activity of Eugenol, bis-Eugenol, and clove essential oil: an in vitro study. ACS omega, 10(28), 31033-31045.

[31] Pochapski, D. J., dos Santos, C. C., Leite, G. W., Pulcinelli, S. H., & Santilli, C. V. (2021). Zeta Potential and Colloidal Stability Predictions for Inorganic Nanoparticle Dispersions: Effects of Experimental Conditions and Electrokinetic Models on the Interpretation of Results. Langmuir, 37(45), 13379–13389. https://doi.org/10.1021/acs.langmuir.1c02056
[32] Queiroz, E. F., Guillarme, D., & Wolfender, J. L. (2024). Advanced high-resolution chromatographic strategies for efficient isolation of natural products from complex biological matrices: from metabolite profiling to pure chemical entities. Phytochemistry Reviews, 23(5), 1415-1442.
[33] Said, R. P., Gawad, J. B., Kalaskar, M., Gurav, N., & Beldar, V. G. (2025). Isolation, Fractionation, and Purification of Natural Products. Pharmacognosy and Phytochemistry: Principles, Techniques, and Clinical Applications, 207-234.
[34] Sharma, M., Bharti, S., Goswami, A., & Mallubhotla, S. (2023). Diversity, antimicrobial, antioxidant, and anticancer activity of culturable fungal endophyte communities in Cordia dichotoma. Molecules, 28(19), 6926.
[35] Skoog, D. A., Holler, F. J., & Crouch, S. R. (2014). Principles of Instrumental Analysis (6th ed.). Cengage Learning, Boston, USA
[36] Stuart, B. H. (2004). Infrared spectroscopy: Fundamentals and applications. John Wiley & Sons.
[37] Sun, Y., and Xia, Y. (2002). Shape-controlled synthesis of gold and silver nanoparticles. Science, 298(5601), 2176–2179.
[38] Ulanowska, M., & Olas, B. (2021). Biological properties and prospects for the application of Eugenol—a review. *International journal of molecular sciences*, *22*(7), 3671.
[39] Vermes, I., Haanen, C., Steffens-Nakken, H., Reutelingsperger, C. (1995). A novel assay for apoptosis: Flow cytometric detection of phosphatidylserine expression on early apoptotic cells using fluorescein-labelled Annexin V. Journal of Immunological Methods, 184(1), 39–51. https://doi.org/10.1016/0022-1759(95)00072-I
[40] Williams, D. B., and Carter, C. B. (2009). Transmission Electron Microscopy: A Textbook for Materials Science. Springer, New York, USA.
[41] Yang, X.-H., Sladek, T. L., Liu, X., Butler, B. R., Froelich, C. J., & Thor, A. D. (2001). Reconstitution of caspase 3 sensitizes MCF-7 breast cancer cells to doxorubicin- and etoposide-induced apoptosis. Cancer Research, 61(1), 348–354.
[42] Yun, S.-M., Lee, M.-H., Lee, K.-J., Ku, H.-O., Son, S.-W., & Joo, Y.-S. (2010). Quantitative analysis of Eugenol in clove extract by a validated HPLC method. Journal of AOAC International, 93(6), 1806–1810. https://doi.org/10.1093/jaoac/93.6.1806